Environmental Science: Atmospheres

ROYAL SOCIETY OF CHEMISTRY

PAPER

View Article Online
View Journal | View Issue

Cite this: *Environ. Sci.: Atmos.*, 2026, **6**, 565

Quantifying sensitivity of $PM_{2.5}$ mass to ammonia and nitrate availability in Hong Kong based on four-year hourly measurements

Zijing Zhang [a] and Jian Zhen Yu *[ab]

Ammonium and nitrate are major components of $PM_{2.5}$, and their fractional contributions to urban $PM_{2.5}$ in China have increased in recent years, largely due to successful sulfate reductions. Owing to their semi-volatile nature, ammonium and nitrate in $PM_{2.5}$ are strongly affected by gas–particle partitioning, which depends on temperature, relative humidity, and the ionic composition of $PM_{2.5}$. Quantifying the sensitivity of $PM_{2.5}$ mass to precursor availability under locale-specific atmospheric conditions is therefore essential for air quality management. In this study, we analyzed four years (2013–2017) of hourly concentrations of inorganic ions and their gaseous precursors at an urban site in Hong Kong. We estimated aerosol water content (AWC) and aerosol pH and conducted a detailed seasonal analysis. Our results revealed distinct sensitivities of $PM_{2.5}$ to ammonia and nitrate availability, modulated by aerosol pH and AWC. In fall, sulfate-dominated $PM_{2.5}$ exhibited low sensitivity to HNO_3, while in winter, increased partitioning ratios led to higher $PM_{2.5}$ sensitivity to HNO_3. Quantitative assessment showed that reductions in water-soluble inorganic PM were proportional to decreases in total nitrate (TNO_3, including gaseous HNO_3 and particulate nitrate) and sulfate, but exhibited a parabolic relationship with reductions in total ammonia (TNH_3, including gaseous NH_3 and particulate ammonium). As TNH_3 levels are further reduced, the sensitivity of $PM_{2.5}$ to NH_3 would increase. Our findings highlight the importance of synergistic reduction of NH_3 and NO_x emissions in effectively mitigating $PM_{2.5}$ pollution. This analysis provides valuable insights to inform the development of targeted, integrated air quality management strategies for urban environments.

Received 15th September 2025
Accepted 4th February 2026

DOI: 10.1039/d5ea00114e

rsc.li/esatmospheres

Environmental significance

Urban $PM_{2.5}$ is increasingly dominated by semi-volatile nitrate and ammonium, challenging one-size-fits-all precursor control. We show why local thermodynamics matter using four years of hourly observations in Hong Kong. We constrain aerosol pH and water and quantify $PM_{2.5}$ sensitivity to precursor availability. $PM_{2.5}$ composition is under "ammonium-rich" regime with substantial NH_4NO_3, and the sensitivity to TNO_3 is higher in winter than fall. Water-soluble inorganic PM falls linearly with total nitrate and sulfate but nonlinearly with total ammonia, yielding larger marginal benefits as NH_3 declines. Therefore, synergistic NH_3–NO_x controls, tuned to season, would offer efficient $PM_{2.5}$ reductions in Hong Kong and analogous urban environments.

1. Introduction

Fine particulate matter ($PM_{2.5}$) adversely affects human health, contributing to respiratory diseases and cardiovascular diseases. Secondary inorganic aerosols (SIAs), including sulfate, ammonium, and nitrate, constitute a major portion of $PM_{2.5}$ worldwide and are therefore central to air quality management and public health. In Hong Kong, SIA species account for over 40% of ambient $PM_{2.5}$ mass.[1–3] Over the years, the composition of $PM_{2.5}$ in Hong Kong has changed markedly in response to emission controls targeting SIA precursor gases. For example, SO_2 emissions from public electricity generation and navigation decreased by around 40% and 50%, respectively, from 2013 to 2017.[4] Consistent with these reductions, annual $PM_{2.5}$ and sulfate concentrations at the urban Tsuen Wan site in Hong Kong showed a clear decline from 2013 to 2017, as documented by Chow *et al.*[2] In comparison, nitrate concentrations based on filter samples remained roughly stable from 2013 to 2016 and increased in 2017, while ammonium concentrations showed minimal interannual variability. Consequently, NH_4^+ and NO_3^- have taken up an increasing mass fraction of $PM_{2.5}$ in Hong Kong. Nitrate forms *via* atmospheric oxidation of NO_x; following stricter vehicle-emission controls, nitrate levels declined notably from 2008 to 2013 in Hong Kong.[2] Recent studies further suggest that ammonia abatement can be a cost-effective lever for PM

[a]*Division of Environment and Sustainability, Hong Kong University of Science and Technology, Clearwater Bay, Kowloon, Hong Kong. E-mail: jian.yu@ust.hk*
[b]*Department of Chemistry, Hong Kong University of Science and Technology, Clearwater Bay, Kowloon, Hong Kong*

reduction, with benefit-to-cost ratios as high as 4.6.[5,6] Given ongoing NO_x controls and the substantial potential for NH_3 emission reductions—particularly from agriculture in mainland China—both NO_x and NH_3 remain key considerations for formulating strategies to further lower $PM_{2.5}$ in Hong Kong.

In Hong Kong, major NO_x sources in 2017 included public electricity generation (37%), marine navigation (27%), and road transport (20%).[4] Ammonia emissions are dominated globally by agriculture (livestock and nitrogen fertilizer use),[7–9] and China is a recognized hotspot due to intensive agricultural activities.[8,10] Additional NH_3 sources include urban transport and certain industrial processes.[8,9] Vehicular NH_3—produced by catalytic aftertreatment chemistry—can be important locally in Hong Kong given high traffic volumes, with emission rates dependent on vehicle technology, operating conditions, and catalyst age.[11,12] Ammonia readily partitions into the particle phase as ammonium sulfate and ammonium nitrate; the abundant NH_3 often yields a strong correlation between sulfate and ammonium in Hong Kong.[2] Although sulfate remains the dominant inorganic $PM_{2.5}$ component on average, nitrate frequently dominates during pollution episodes, especially in fall and winter. Suburban observations indicate that nitrate episodes often occur under "ammonium-rich" conditions, highlighting the increasing role of ammonium during such events.[13] These findings imply that reducing the availability of both HNO_3 and NH_3 would help curb episodic $PM_{2.5}$, especially during fall and winter.

The abundance of ammonium and nitrate in the particle phase is governed by their thermodynamic equilibrium with gaseous NH_3 and HNO_3 and is strongly modulated by aerosol acidity (pH). As a result, equal total ammonia ($TNH_3 = NH_3 + NH_4^+$, *i.e.*, combined gaseous NH_3 and PM NH_4^+) or total nitrate ($TNO_3 = HNO_3 + NO_3^-$, combined gaseous HNO_3 and PM NO_3^-) can yield different particle-phase NH_4^+ and NO_3^- concentrations depending on aerosol pH. Therefore, the effectiveness of reducing PM mass per unit decrease in TNH_3 or TNO_3 depends on acidity; quantifying this effectiveness, hereafter referred to as PM mass sensitivity, is essential for designing efficient control strategies.

Aerosol pH exhibits significant spatial and temporal variability, influenced by PM composition and mass concentration, aerosol water content (AWC), relative humidity (RH), and temperature. Reported pH during pollution episodes in northern China (*e.g.*, Tianjin and Beijing) typically ranges from ~4 to 5.4,[14–17] decreasing to below 3 during cleaner periods with reduced dust, alkaline species, and AWC.[17] In the Yangtze River Delta (YRD) region, Shanghai's aerosol pH decreased from 3.30 ± 0.58 in 2011 to 3.06 ± 0.58 in 2019.[18] In the Pearl River Delta region, for example Hong Kong, average aerosol pH is far more acidic (*e.g.*, −0.03 ± 0.77).[19] Similarly low pH (~0–1) has been observed in the southeastern United States despite >60% sulfate reductions from 1999 to 2014.[20] Given the central role of pH in controlling gas–particle partitioning and its variability, updated assessments for recent years are needed to inform control policy.

The effect of aerosol pH, temperature and relative humidity on the gas–particle partitioning ratio of nitrate and ammonium was intensively investigated and established in earlier studies.[21–25] As the partitioning ratios $\varepsilon(NO_3^-)$ and $\varepsilon(NH_4^+)$ are functions of pH, temperature and AWC, Nenes *et al.*[26] recently developed a thermodynamic regime framework that classifies PM response to NH_3 and HNO_3 availability. Four regimes—Insensitive, HNO_3-Sensitive, NH_3-Sensitive, and Both-Sensitive—are defined by threshold partitioning ratios in the framework. For example, when $\varepsilon(NO_3^-)$ exceeds a threshold (*e.g.*, 0.1, indicating >10% of TNO_3 in the particle phase), the conditions are classified as "HNO_3-Sensitive"; if both $\varepsilon(NO_3^-)$ and $\varepsilon(NH_4^+)$ exceed the threshold vale, the system is Both-Sensitive. Applying this framework to observations enables identification of dominant controlling precursors. For instance, analysis in Tianjin by Zhao *et al.*[27] indicated predominant HNO_3 sensitivity, with NH_3 sensitivity increasing with sulfate due to ammonium sulfate formation.

Here, using four years of hourly SIA and related measurements (2013–2017), we quantified trends and variability in aerosol pH in Hong Kong and applied the Nenes framework to assess how $PM_{2.5}$ responds to changes in NH_3 and HNO_3 availability under varying PM loadings and across seasons. We further examine nitrate formation under both ammonium-poor and ammonium-rich regimes. More importantly, we quantified $PM_{2.5}$ mass responses to incremental reductions in TNH_3 and TNO_3 in a real-world urban environment through simulations, providing a predictive framework for designing effective control strategies. Our results inform control strategies targeting NH_3 and HNO_3 to mitigate $PM_{2.5}$ in Hong Kong and offer broader insights for urban regions facing analogous challenges.

2. Methods

2.1 Data sources

Sampling was conducted at the Yuen Long Air Quality Monitoring Station (YL AQMS; 22°26′48″ N, 114°01′21.7″ E), an urban site within the Hong Kong Air Quality Monitoring Network. Measurements spanned July 2013 to June 2017, with a suspension from September 2015 to August 2016. The YL site is characterized by heavy nearby traffic and is therefore considered to be under notable influence of vehicular emissions. Supporting evidence includes distinct diurnal patterns of NH_3 and NH_4^+ at YL compared with suburban sites (Fig. S1 and S2).

Hourly concentrations of water-soluble inorganic ions in $PM_{2.5}$ (Na^+, NH_4^+, K^+, Mg^{2+}, Ca^{2+}, Cl^-, NO_3^-, and SO_4^{2-}) and corresponding semi-volatile gases (NH_3, HNO_3, and HCl) were measured using a Monitor for AeRosols and Gases in ambient Air (MARGA 2S ADI2080, Metrohm Applikon). Gaseous species were collected in a wet rotating denuder (WRD) using H_2O_2 as the absorbent, while particles were dissolved in a steam-jet aerosol collector (SJAC). The resulting solutions were analyzed by ion chromatography, with each sample calibrated using an internal LiBr standard. Data validation procedures for MARGA are provided in Section S1. Concurrently, hourly $PM_{2.5}$ mass was measured with a Synchronized Hybrid Ambient Real-time Particulate Monitor (SHARP 5030, Thermo Scientific), and NO_x data were obtained from the Hong Kong Environmental Protection Department (HKEPD) air quality database.

2.2 Calculation of aerosol pH and aerosol water content

Because aerosol pH is not directly measurable, we estimated it using ISORROPIA-II,[28] which calculates the equilibrium partitioning of inorganic gases and aerosols and outputs aerosol water content of inorganic species (W_i) and hydrogen ion concentration $c(H^+)$. We ran ISORROPIA-II in forward mode using measured total concentrations of semi-volatile species ($HNO_3 + NO_3^-$, $NH_3 + NH_4^+$, $HCl + Cl^-$) as inputs, which reduces sensitivity to measurement errors compared with reverse mode.[29,30] Because the model computes the equilibrium partitioning of NH_3/NH_4^+ and HNO_3/NO_3^-, its predications were compared with MARGA measurements to assess the performance of model calculation. Overall, the model reproduced the measurements from MARGA, indicating reliable model predictions in our study (Fig. S4). When the RH decreases below the deliquescence RH, the aerosol would not crystalize immediately but instead constitute a supersaturated aqueous solution.[15,31] Considering Hong Kong's wet climate with average RH as high as 64% ± 14% in our study, the calculation was based on metastable state assumption (*i.e.*, all salts in the aqueous phase without precipitated salt). Aerosol pH was computed as:

$$\mathrm{pH} = -\lg\frac{\gamma_{H^+} \times c(H^+) \times 1000}{W} = -\lg\frac{\gamma_{H^+} \times c(H^+) \times 1000}{W_i} \quad (1)$$

where γ_{H^+} is the H^+ activity coefficient (assumed unity), $c(H^+)$ is in μmol m^{-3}, W is the total AWC in μg m^{-3}, and W_i is the AWC attributable to inorganic species (μg m^{-3}).[29] We set $W = W_i$, following prior studies showing that using inorganic AWC alone provides a reasonable estimate of aerosol pH, even when organics constitute a fraction as large as 70% of $PM_{2.5}$ mass.[29,31]

2.3 Determining PM sensitivity to TNO_3 and TNH_3

$PM_{2.5}$ responses to precursor availability are governed by gas–particle partitioning thermodynamics. For a given TNO_3, a higher nitrate partitioning ratio $\varepsilon(NO_3^-)$ yields a larger fraction of TNO_3 in the particle phase and thus a greater PM mass response to incremental HNO_3. Analogously, PM sensitivity to TNH_3 scales with the ammonium partitioning ratio $\varepsilon(NH_4^+)$. To maintain comparability with prior studies, we adopt a partitioning threshold of 0.1. For example, $\varepsilon(NO_3^-) > 0.1$ indicates that, for a unit increase in HNO_3, 10% of it partitions to the particle phase, producing a meaningful PM mass response; we therefore classify $\varepsilon(NO_3^-) > 0.1$ as HNO_3-Sensitive and $\varepsilon(NH_4^+) > 0.1$ as NH_3-Sensitive.[26,27]

Gaseous HNO_3 is in equilibrium with particulate nitrate through dissolution of HNO_3 and acid dissociation. With these two processes of equilibrium, the theoretical $\varepsilon(NO_3^-)$ can be calculated using eqn (2):[26,29]

$$\varepsilon(NO_3^-) = \frac{H_{HNO_3} K_{n1} WRT}{\gamma_{NO_3^-}\gamma_{H^+} \times 10^{-\mathrm{pH}} + H_{HNO_3} K_{n1} WRT} \quad (2)$$

where H_{NO_3} is the Henry's law constant of HNO_3, K_{n1} is the acid dissociation constant of HNO_3, W is the aerosol water content, R is the ideal gas constant, T is the measured ambient temperature, and $\gamma_{NO_3^-}$ and γ_{H^+} are the activity coefficients of NO_3^- and H^+ from ISORROPIA-II. $\varepsilon(NO_3^-)$ is a sigmoid function of aerosol pH and depends on W and T. Similarly, the equilibrium between gaseous NH_3 and particulate NH_4^+ also includes the processes of dissolution and dissociation, and $\varepsilon(NH_4^+)$ can be expressed as eqn (3),[26,29]

$$\varepsilon(NH_4^+) = \frac{\frac{\gamma_{H^+} \times 10^{-\mathrm{pH}}}{\gamma_{NH_4^+}} \frac{H_{NH_3}}{K_a} WRT}{1 + \frac{\gamma_{H^+} \times 10^{-\mathrm{pH}}}{\gamma_{NH_4^+}} \frac{H_{NH_3}}{K_a} WRT} \quad (3)$$

where H_{NH_3} is the Henry's law constant for NH_3, K_a is the acid dissociation constant of NH_4^+, and $\gamma_{NH_4^+}$ is the NH_4^+ activity coefficient. Predicted partitioning ratios from ISORROPIA-II were found to be in good agreement with measured data.[29]

We applied the thermodynamic regime framework of Nenes *et al.*[26] to classify each hourly observation into four sensitivity regimes, namely "HNO_3-Sensitive", "NH_3-Sensitive", "Both-Sensitive", and "Insensitive", based on $\varepsilon(NO_3^-)$ and $\varepsilon(NH_4^+)$, which are functions of pH, W, and T. To examine how PM loadings and meteorology modulate sensitivity, we further stratified the data by $PM_{2.5}$ concentration and by season. This stratification enables evaluation of regime frequency and PM response across contrasting conditions.

3. Results & discussion

3.1 Interannual and seasonal variability of pollutant concentrations

Monthly averages (Fig. 1) show consistent seasonality for $PM_{2.5}$, TNO_3, and TNH_3, with maxima in fall–winter and minima in summer. From 2013 to 2016, wintertime $PM_{2.5}$ and NO_x decreased by approximately 40% and 33%, respectively (Table 1). TNO_3 declined by 37% over the same period, consistent with reductions in NO_x emissions. However, TNH_3 concentration only decreased by 7.1%, much less than other compounds. Even in summer (the least polluted season), $PM_{2.5}$, NO_x, TNO_3, and SO_4^{2-} all exhibited year-on-year decreases, while TNH_3 was even higher in 2016 than 2013. This divergence indicates that while controls on SO_2 and NO_x were effective, ammonia emissions have not been effectively controlled, and its availability remained relatively stable. Notably, as $PM_{2.5}$ concentrations declined, the fractional contribution of SIA to $PM_{2.5}$ increased, highlighting a growing relative importance of ammonium and nitrate. This shift underscores the need to complement ongoing SO_2 and NO_x controls with strategies targeting NH_3 and HNO_3 precursors, particularly to address semi-volatile SIA components that become more influential at lower PM loadings.

3.2 Aerosol pH in Hong Kong

Aerosol pH is a central thermodynamic parameter that influences multiple atmospheric processes. For example, stronger acidity accelerates acid-catalyzed pathways for secondary organic aerosol (SOA) formation from volatile organic compounds (VOCs), and controls the solubility of SO_2, NH_3, and HNO_3, thereby regulating aqueous-phase sulfate production and the gas–particle partitioning of nitrate and ammonium.[32] Because in Hong Kong both SOA and SIA constitute substantial

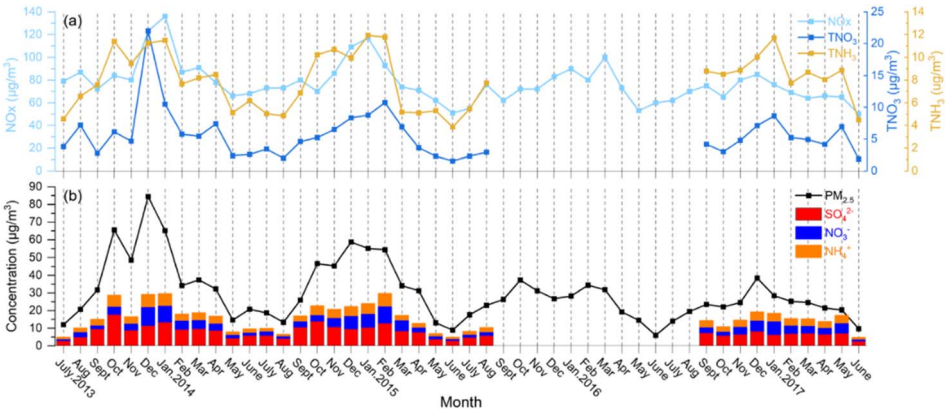

Fig. 1 Monthly average concentration data of select constituents for the period of July 2013–June 2017. (a) NO_x, TNO_3 and TNH_3. (b) $PM_{2.5}$, $PM_{2.5}$-associated SO_4^{2-}, NO_3^-, and NH_4^+. No measurements are available for the period of September 2015–August 2016.

fractions of $PM_{2.5}$, aerosol pH fundamentally modulates secondary aerosol formation rates and mechanisms and is a key factor in understanding variability in the city's PM levels.[33,34]

Fig. 2 shows a pronounced diurnal cycle in aerosol pH during all seasons. The method of dividing the four seasons was based on upper-level wind, dew point and sea level pressure.[35] Aerosol pH was the lowest in the afternoon and the highest around dawn; afternoon values were typically 0.6–0.8 units lower than the values at dawn. This diurnal variability was comparable to interannual differences despite substantial compositional changes over the years (Fig. 1), indicating that meteorology (RH and temperature) dominates pH variability. Consistently, the pH diurnal cycle tracked RH and was anti-correlated with temperature (Fig. S5 and S6). Seasonally, winter exhibited the highest pH despite having the lowest RH, which would ordinarily depress pH by reducing aerosol water. This contrast suggests that temperatures dominate the seasonal control on aerosol pH in Hong Kong, consistent with observations in Shanghai.[18]

Over the five-year period, aerosol pH remained relatively stable even as sulfate and NO_x concentrations declined markedly, paralleling trends observed in the southeastern United States.[20] However, summertime pH in Hong Kong (1.5–3.0) was higher than that typically observed in the southeastern U.S. (0–1). The comparatively lower acidity in Hong Kong implies weaker acid-catalyzed uptake of certain VOC oxidation products (*e.g.*, IEPOX from isoprene oxidation) and slower acid-driven heterogeneous reactions,[36,37] while favoring faster aqueous-phase sulfate production from SO_2. Consequently, Hong Kong's higher pH environment likely enhances inorganic sulfate formation but suppresses SOA yields from acid-dependent pathways, increasing the relative contribution of inorganic aerosol compared with regions characterized by more acidic particles.

3.3 Impact of key factors on PM sensitivity across seasons

The thermodynamic regime framework indicates that PM mass sensitivity to TNO_3 and TNH_3 is governed by AWC and aerosol pH. Because higher PM loadings enhance water uptake and shift composition, both AWC and pH are indirectly modulated by PM mass and species such as sulfate and ammonium. We therefore examined how $PM_{2.5}$ mass, sulfate, and TNH_3 influence sensitivity across seasons.

3.3.1 Effect of PM mass. In spring, most observations fell within the "Both-Sensitive" regime (Fig. 3a), indicating concurrent sensitivity to TNO_3 and TNH_3. Under low PM conditions, points clustered near regime boundaries, implying weak sensitivity to both precursors. As PM mass increased, AWC would be higher, favoring the partitioning of both HNO_3 and NH_3, thus the sensitivity to TNO_3 and TNH_3 would be strengthened. In summer, at low PM, the regime distribution resembled that of spring (Fig. 3b). With increasing PM, data shifted toward "Both-Sensitive" and "NH_3-Sensitive" regimes, indicating that high-PM summer days are consistently "NH_3-Sensitive". In fall, the distribution was dominated by "Both-

Table 1 Summer and winter average concentrations of major species in 2013, 2014 and 2016

	$PM_{2.5}$ (μg m^{-3})	NO_x (ppb)	TNO_3 (μg m^{-3})	TNH_3 (μg m^{-3})	SO_4^{2-} (μg m^{-3})
2013-Summer	22.7	42.0	4.5	6.4	6.2
2013-Winter	54.2	59.3	10.2	9.9	11.2
2014-Summer	23.2	37.8	3.0	5.8	6.6
2014-Winter	58.3	56.6	9.2	10.9	10.8
2015-Summer	16.3	32.1	2.3	5.8	4.4
2015-Winter	—	—	—	—	—
2016-Summer	19.6	34.2	3.3	7.1	5.6
2016-Winter	32.7	41.4	6.3	9.2	7.7

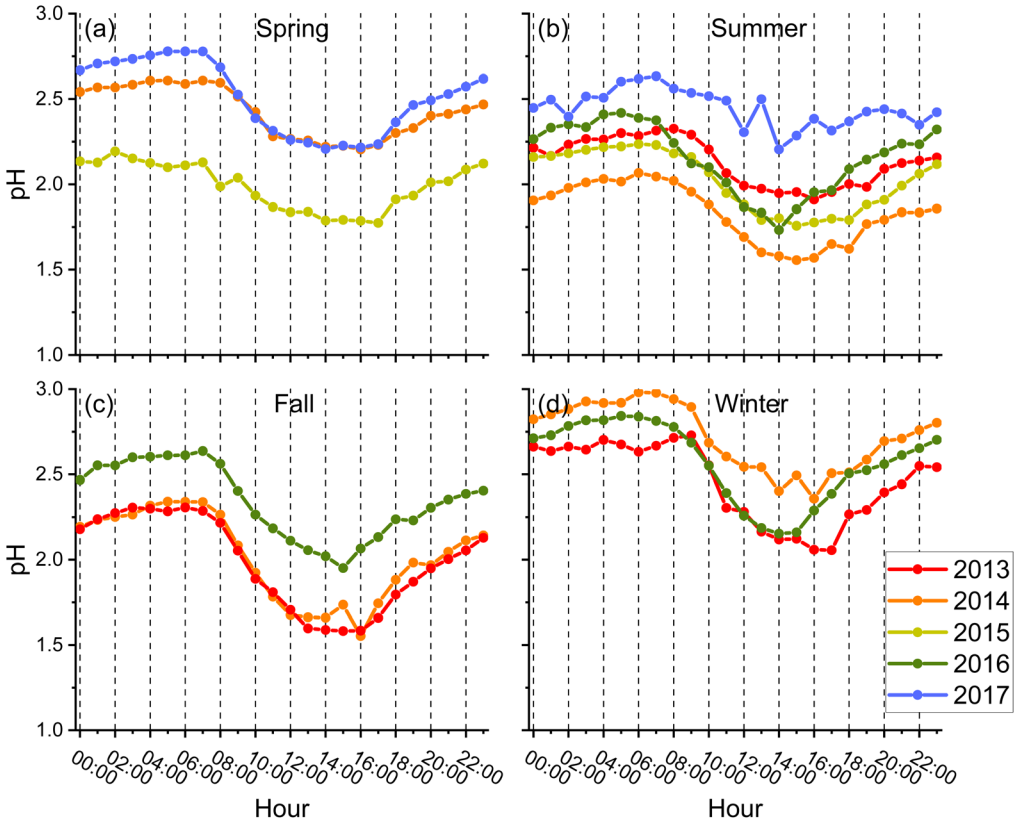

Fig. 2 Season-specific diurnal variation of aerosol pH: (a) spring, (b) summer, (c) fall, and (d) winter.

Sensitive" and "NH_3-Sensitive" regimes (Fig. 3c). Increasing PM pushed points toward the lower-right of the regime space, signifying enhanced NH_3 sensitivity under polluted conditions. In winter, most observations were in the "Both-Sensitive" regime (Fig. 3d), consistent with enhanced NO_3^- and NH_4^+ partitioning at lower temperatures. Unlike other seasons, the distribution showed no clear moving trend across PM gradients, suggesting a more uniform sensitivity state in winter. The weaker influence of PM mass to AWC reflected the lower hygroscopicity of the dominant pollutants during winter. The seasonal contrasts mostly reflected differences in PM composition and meteorology.

To contextualize high-loading conditions, we adopted the 24-hour $PM_{2.5}$ standard of 50 μg m^{-3} (WHO interim target-2),[38] as used in Hong Kong's Air Quality Objectives for 2022–2025, to define polluted conditions. Exceedances occurred more frequently in fall and winter (Fig. 3), so subsequent analyses of polluted cases focus on these seasons (Fig. S7). Fall polluted cases exhibited stronger sensitivity to TNH_3 than to TNO_3 (Fig. S8). In winter, sensitivity to TNO_3 intensified relative to fall, while NH_3 sensitivity remained. Elevated sulfate was associated with increased NH_3 sensitivity in both fall and winter. This mirrors the effect of higher PM in fall but contrasts with winter, where increases in PM did not shift regimes as distinctly. Overall, these patterns suggest that sulfate is a primary driver of NH_3 sensitivity in fall, whereas nitrate assumes a comparatively greater role in winter, consistent with colder temperatures favoring partitioning of HNO_3 and NH_3 to the particle phase.

3.3.2 Impact of sulfate. Regime plots stratified by sulfate concentration show a consistent sulfate-driven enhancement of sensitivity across all seasons (Fig. 4). As sulfate increases, points shift systematically toward the lower-right of the regime space, indicating stronger NH_3 sensitivity and greater NH_4^+ partitioning. This behavior reflects two concurrent effects of sulfate. First, sulfate protonation increases aerosol acidity, which thermodynamically favors uptake of gaseous NH_3 into the particle phase but lowers the partitioning ratio of nitrate. Second, sulfate's hygroscopicity elevates AWC, promoting gas-to-particle conversion of NH_3 and HNO_3. Although previous studies showed that aerosol pH was insensitive to sulfate concentration because higher AWC offsets the effect of sulfate protonation,[39] higher sulfate still contributes to the lower pH in Hong Kong. Therefore, the sensitivity to TNH_3 was more greatly influenced by sulfate concentration while the effect on the sensitivity to TNO_3 was partly offset. These results indicate that sulfate acts as a primary modulator of NH_3-driven PM responses in all seasons.

3.3.3 Impact of TNH_3. Stratification by TNH_3 reveals seasonally distinct controls on sensitivity to TNH_3 and TNO_3 (Fig. 5). In spring and winter, higher TNH_3 shifts points toward the upper-right portion of the regime map, increasing sensitivity to TNO_3 through enhanced formation of NH_4NO_3. Summer displays a predominantly horizontal displacement into the "Both-Sensitive" regime, indicating concurrent increases in sensitivity to both TNH_3 and TNO_3. In contrast, in fall, increasing TNH_3 mirrors the sulfate effect by primarily strengthening NH_3 sensitivity, with limited impact on HNO_3 sensitivity.

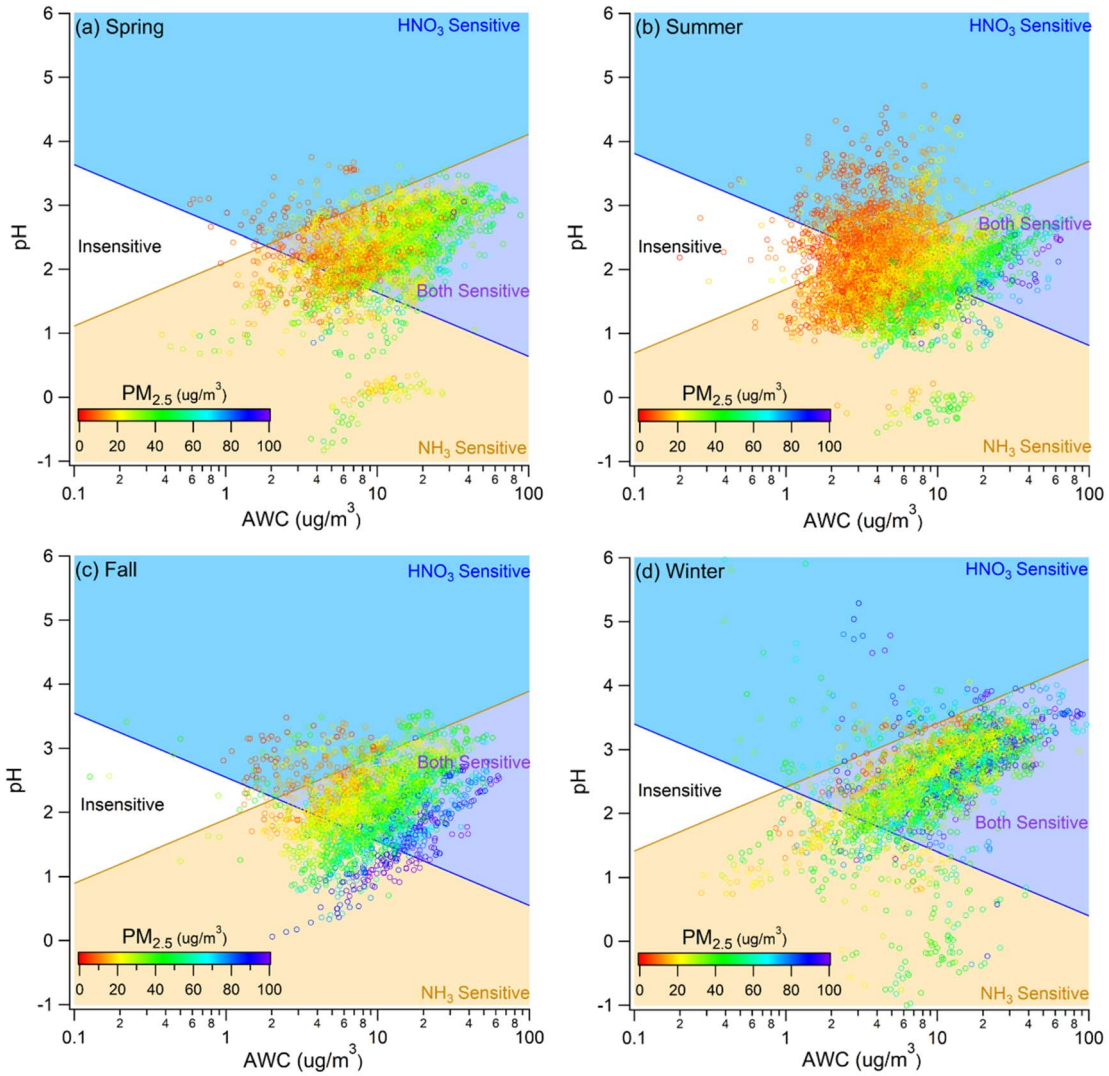

Fig. 3 Sensitivity regime plots for (a) spring, (b) summer, (c) fall, and (d) winter. The data points are colored by PM concentration using a common scale.

These seasonal differences are consistent with composition-dependent thermodynamics. During winter, elevated TNO_3 facilitates NH_4NO_3 formation when TNH_3 is abundant, so PM mass becomes more responsive to additional HNO_3. In fall, comparatively lower TNO_3 constrains NH_4NO_3 formation, limiting the influence of TNH_3 on HNO_3 sensitivity. Nevertheless, higher TNH_3 increases AWC and reduces particle-phase ammonia scarcity, both of which favor NH_3 partitioning and elevate $\varepsilon(NH_4^+)$. Consequently, regardless of season, increases in TNH_3 enhance NH_3 sensitivity, while the concurrent effect on HNO_3 sensitivity depends on the availability of total nitrate and seasonal thermodynamic conditions.

3.4 Nitrate formation under ammonium-rich and ammonium-poor regimes

In the thermodynamic equilibrium state, the particulate ammonium concentration constrains the simultaneous formation of ammonium sulfate and ammonium nitrate. Significant concentrations of particulate nitrate (as NH_4NO_3) are thermodynamically sustainable only when the molar amount of aerosol-phase ammonium exceeds that required to associate with sulfate.[40] The "excess ammonium" is defined as $[NH_4^+] - K \times [SO_4^{2-}]$, where K is an empirical criterion molar ratio of ammonium to sulfate.[41] Following established practice,[42,43] K is obtained as the x-intercept of the correlation between $[NO_3^-]/[SO_4^{2-}]$ and $[NH_4^+]/[SO_4^{2-}]$. Conditions with $[NH_4^+]/[SO_4^{2-}] > K$, which means that the excess ammonium is greater than zero, are classified as "NH_4^+-rich", and those with $[NH_4^+]/[SO_4^{2-}] < K$ as "NH_4^+-poor". This particle-phase classification provides a diagnostic for the thermodynamic state resulting from the partitioning of TNH_3 and TNO_3. The "NH_4^+-rich" regime indicates that, given the ambient TNH_3, TNO_3, and thermodynamic conditions (AWC, pH, T), the system favors the formation of particulate nitrate. Its occurrence is therefore modulated by factors such as AWC, which shifts the partitioning equilibrium.

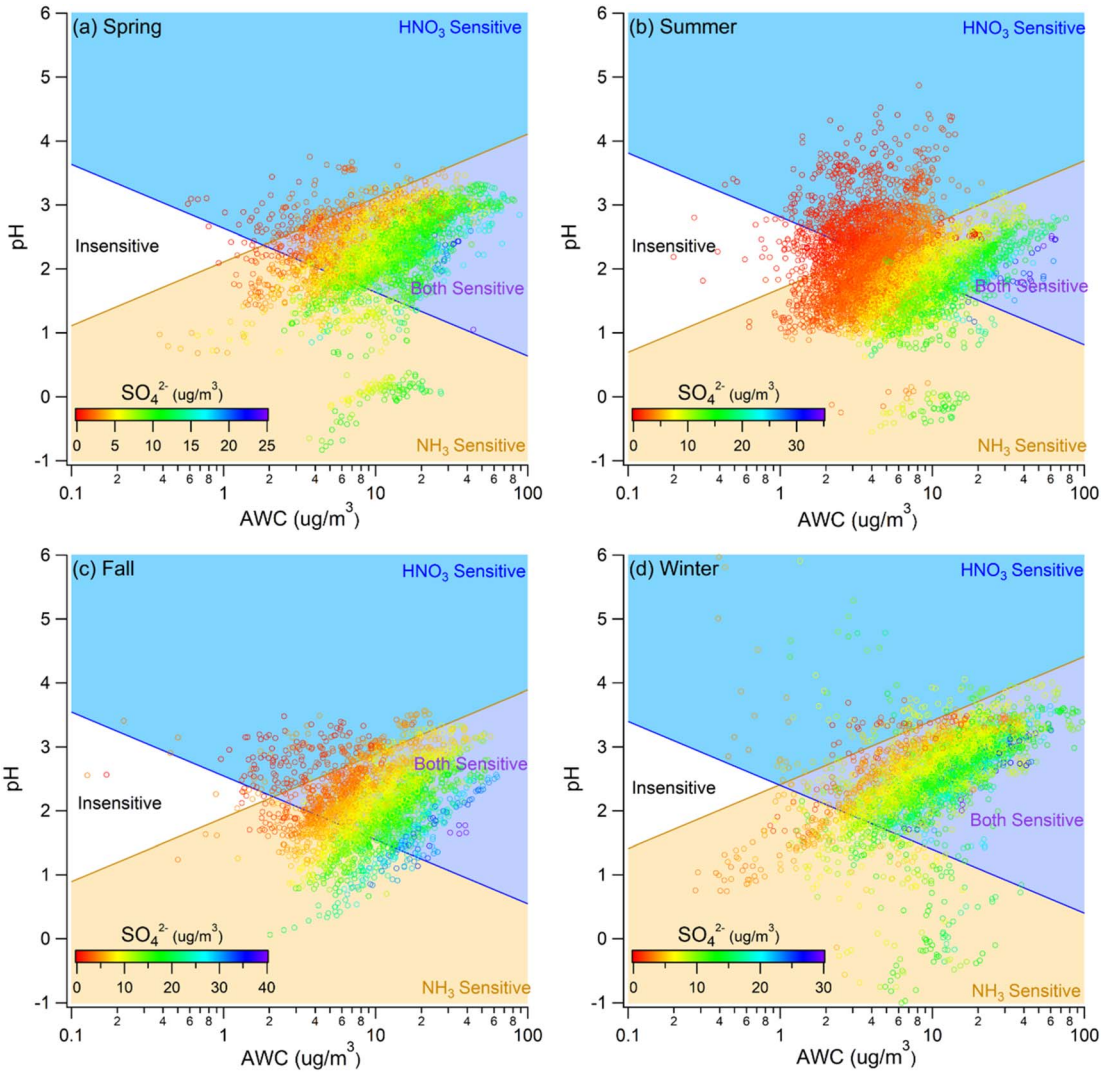

Fig. 4 Sensitivity regime plots colored by sulfate concentration for (a) spring, (b) summer, (c) fall, and (d) winter.

The classification of regimes is primarily controlled by the relative emission strengths and transport of precursors, and the regime shift is a more fundamental change in aerosol composition that typically occurs over longer timescales. Therefore, here we separate the data by seasons. Season-resolved correlation plots indicate that NH_4^+-rich conditions prevail in spring, fall, and winter, whereas NH_4^+-poor conditions occur more frequently in summer (Fig. S9). Linear regressions of $[NO_3^-]/[SO_4^{2-}]$ against $[NH_4^+]/[SO_4^{2-}]$, along with the derived K values for each season, are summarized in Table 2. Note that the value of K is not a universal constant but is influenced by local thermodynamic environment. Its value ranges from 1.58 to 1.78 across seasons, and the seasonal variation in K could be attributed to the variation in non-volatile cations, temperature and RH. For example, temperature can influence the activity coefficients and the equilibrium constant for NH_4NO_3 dissociation, subtly shifting the K value defined by the $[NO_3^-]/[SO_4^{2-}]$ *vs.* $[NH_4^+]/[SO_4^{2-}]$ correlation. The range of K values in our study is consistent with that reported in prior studies.[41,43,44] Importantly, AWC is a key factor influencing this local thermodynamic environment. By affecting the activity coefficients and the equilibrium constant for semi-volatile species such as NH_4NO_3, variations in AWC (driven by RH and inorganic mass) contribute to the observed seasonal shifts in the empirical K value.

Using the season-specific K, we calculated "excess ammonium" and examined its relationship with particulate nitrate. Under "NH_4^+-rich" conditions, excess ammonium strongly correlates with nitrate concentration in all seasons (Fig. 6), supporting the interpretation that NH_4NO_3 forms efficiently when ammonium is available beyond that required to neutralize sulfate. The seasonal slopes of nitrate *versus* excess ammonium ranged from 0.71 to 0.84, indicating that the majority of excess ammonium is present as NH_4NO_3. By contrast, nitrate concentrations remained very low under "NH_4^+ poor" conditions, reflecting the constraint imposed by insufficient ammonium to neutralize nitric acid. Consequently, nitrate-dominated aerosol states primarily occurred in "NH_4^+-

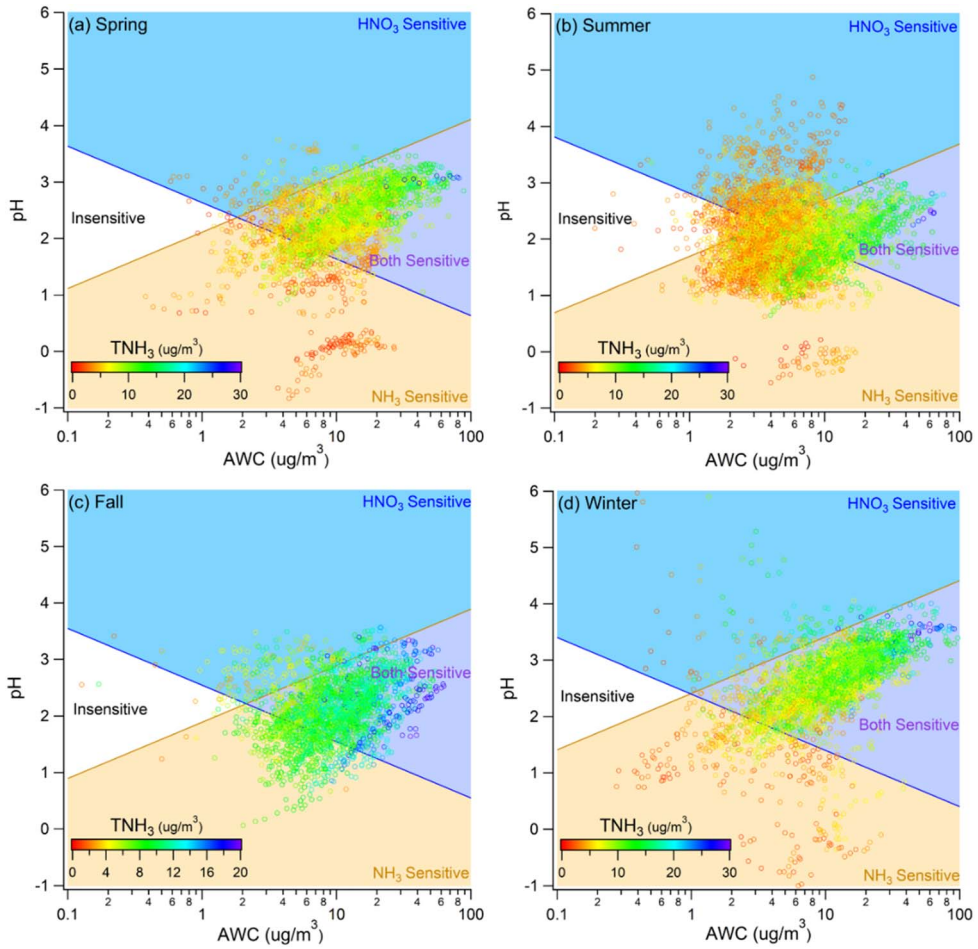

Fig. 5 Sensitivity regime plots colored by TNH_3 concentration for (a) spring, (b) summer, (c) fall, and (d) winter.

Table 2 Season-specific linear regression equations between $[NO_3^-]/[SO_4^{2-}]$ and $[NH_4^+]/[SO_4^{2-}]$ and the K values

Season	Regression equation	K value
Spring	$Y = 0.83X - 1.31$	1.58 ± 0.025
Summer	$Y = 0.91X - 1.62$	1.78 ± 0.030
Fall	$Y = 0.80X - 1.35$	1.69 ± 0.034
Winter	$Y = 0.85X - 1.38$	1.62 ± 0.020

rich" regimes, while "NH_4^+-poor" conditions at the YL site were generally associated with cleaner periods. Aerosol pH ranged from 0.5 to 4 across all seasons. In the "NH_4^+-rich" regime, aerosol pH increased with nitrate concentration, consistent with the thermodynamic expectation that higher pH favors nitrate partitioning into the particle phase. Differently, aerosol pH was more influenced by crustal cations under "NH_4^+-poor" regime. On average, aerosol pH was 0.2 to 0.6 units higher in the "NH_4^+-rich" regime due to the higher ammonia abundance (Table 3). This analysis underscores that substantial nitrate formation requires not only high total precursor concentrations but also a thermodynamic state (often characterized by sufficient AWC and higher aerosol pH) that drives TNO_3 into the particle phase.

3.5 Simulation of water-soluble inorganic component (WSIC) reduction in fall and winter

3.5.1 Single-factor sensitivity simulations. Base scenarios were constructed using seasonally average concentrations of water-soluble inorganic components (WSICs) and meteorological parameters for fall and winter (Table 4). We then simulated reductions in TNO_3, sulfate and TNH_3 by scaling each concentration by a factor x from 1.0 to 0.4. For each perturbed scenario, aerosol pH and AWC were computed with ISORROPIA-II, and the corresponding shift of PM sensitivity to TNH_3 and TNO_3 was mapped onto the regime plot (Fig. 7). The concentration of total chloride ($TCl = HCl + Cl^-$) and NVCs constituted a minor mass fraction of $PM_{2.5}$, so their influence on aerosol pH was negligible and is not discussed in this study. For example, in the fall sulfate-reduction simulations, excluding TCl and NVCs from the pH calculation changes aerosol pH by only 0.14 ± 0.05 units.

In fall, the base state lies in the "Both-Sensitive" regime. Reducing TNH_3 rapidly induces rapid decline in HNO_3 sensitivity; an ~40% reduction in TNH_3 shifts the system to the "NH_3-Sensitive" regime. Decreasing sulfate lowers NH_3 sensitivity, consistent with sulfate's role in enhancing acidity and AWC and thereby promoting NH_3 partitioning. An ~60% reduction in sulfate drives the system toward the "HNO_3-

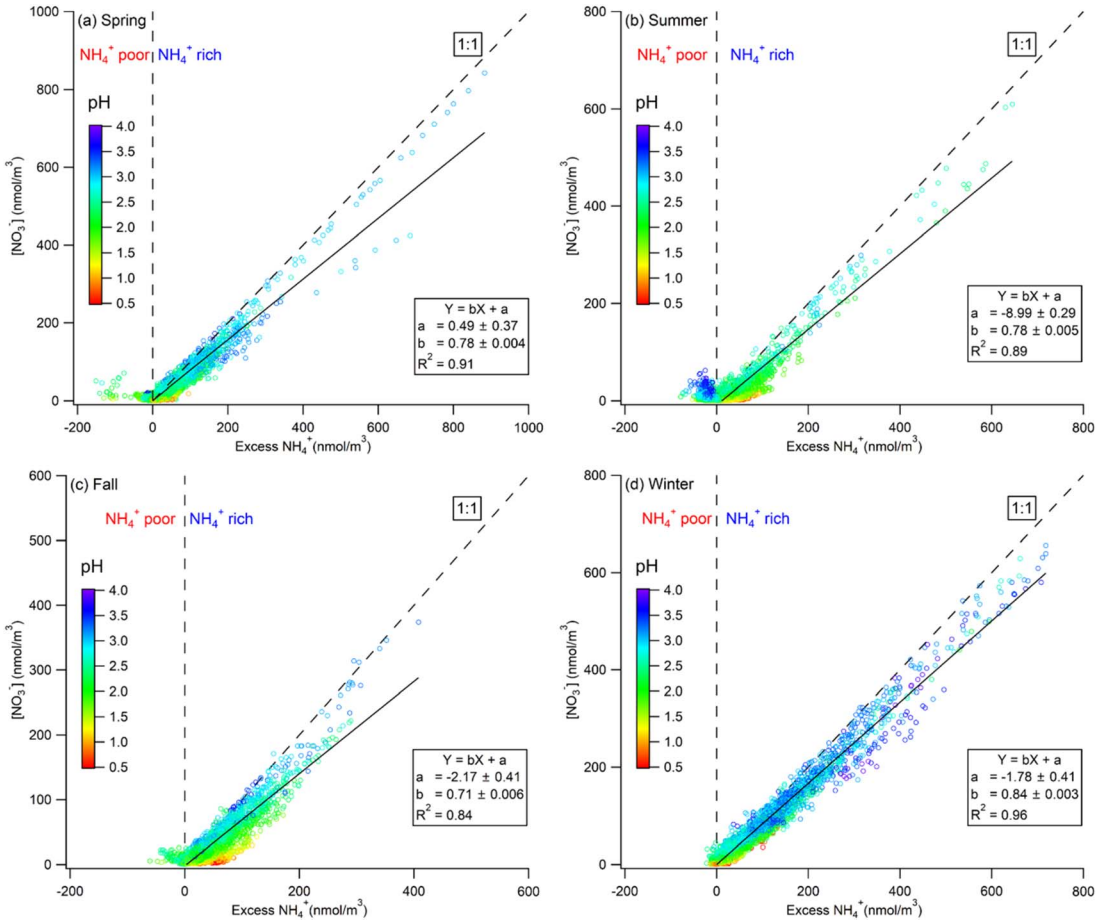

Fig. 6 Correlation plots between nitrate concentration and excess ammonium concentration for (a) spring, (b) summer, (c) fall, and (d) winter with data points colored by aerosol pH.

Table 3 Season-specific average aerosol pH under "NH_4^+-rich" and "NH_4^+-poor" conditions

Season	NH_4^+-rich	NH_4^+-poor
Spring	2.4	2.0
Summer	2.1	1.9
Fall	2.2	1.6
Winter	2.6	2.0

Sensitive" regime. Notably, sulfate reductions have little effect on the degree of HNO_3 sensitivity itself, as points translate largely parallel to the "HNO_3-Sensitive" boundary, confirming limited NH_4NO_3 formation in fall because of constrained TNO_3. In contrast, changes in TNO_3 have negligible influence on pH, AWC, or regime position, indicating weak leverage of nitrate on sensitivity under fall conditions.

Winter shows a similar baseline in the "Both-Sensitive" regime. As in fall, cutting TNH_3 quickly diminishes HNO_3 sensitivity, and pH and AWC remain insensitive to TNO_3 changes. However, sulfate reductions in winter increase HNO_3 sensitivity, with points moving away from the "HNO_3-Sensitive" boundary and penetrating deeper into the "HNO_3-Sensitive" regime. This pattern indicates that ammonium nitrate contributes substantially to PM in winter alongside ammonium sulfate, so lowering sulfate frees ammonium for nitrate formation and accentuates responsiveness to HNO_3.

Using the simulated regime outputs, we further quantified the reductions in WSIC concentrations resulting from decreases in TNO_3, TNH_3, or sulfate and compared the relative efficiencies

Table 4 Seasonal average concentrations of WSICs and meteorology factors in fall and winter[a]

	TNO_3	TNH_3	TCl	SO_4^{2-}	Na^+	K^+	Mg^{2+}	Ca^{2+}	Temp.	RH
Fall	5.0	9.9	0.66	10.9	0.23	0.26	0.04	0.16	25.1	59.8
Winter	8.5	10.0	0.94	9.8	0.32	0.43	0.05	0.18	17.6	55.9

[a] Unit: μg m^{-3} for WSICs, °C for temp. and % for RH.

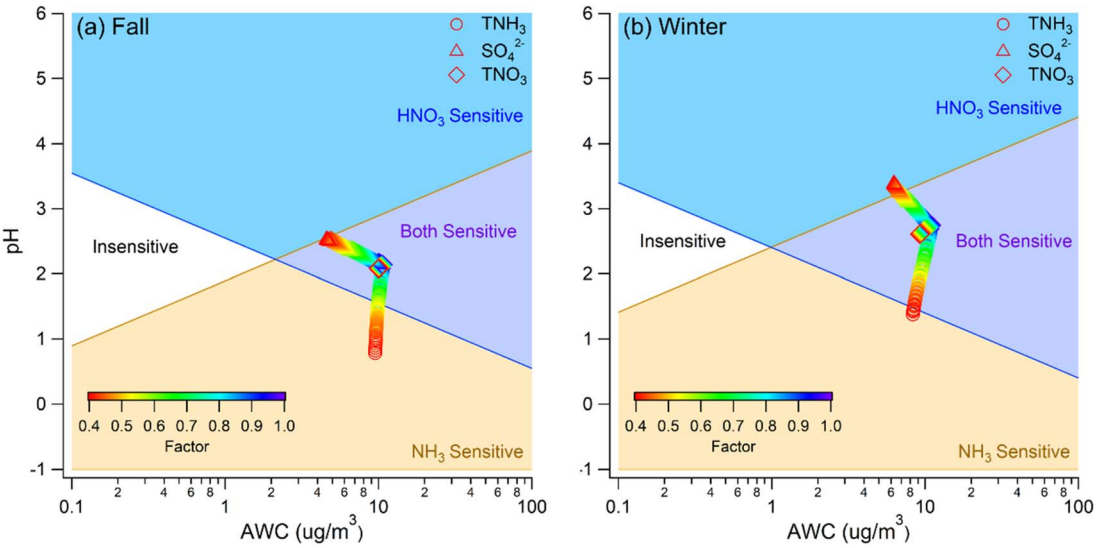

Fig. 7 Changes in PM sensitivity when scaling a single factor from 0.4 to 1.0 during (a) fall and (b) winter. In each panel, the top, middle, and bottom traces correspond to perturbations of SO_4^{2-}, TNO_3, and TNH_3, respectively.

of each control pathway in fall and winter (Fig. 8, red curve). Sulfate abatement is the most effective strategy for reducing WSICs because sulfate is non-volatile and its reductions directly diminish particulate SO_4^{2-} while simultaneously lowering the partitioning of NH_3 to NH_4^+, thereby reducing particle-phase ammonium. Consistent with the regime analysis (Fig. S10 and S11), sulfate controls thus exert compounding benefits on WSICs.

In contrast, TNO_3 reductions have minimal influence on aerosol pH and AWC, so they do not substantially alter ammonia partitioning. Under these conditions, the decrease in SIA attributable to nitrate controls is approximately the reduction in TNO_3 multiplied by the particle-phase nitrate partitioning ratio (Fig. 8, blue curve). TNH_3 reduction would lead to a great increase in $\varepsilon(NH_4^+)$ because of the lowered aerosol pH (Fig. S11). Consequently, TNH_3 reduction would be increasingly efficient as more TNH_3 is reduced, because a larger fraction of TNH_3 would be in the particle phase, producing a characteristic parabolic relationship between WSIC reduction and TNH_3 reduction (Fig. 8, pale yellow curve).

In fall, the effectiveness of reducing TNO_3 or TNH_3 is limited by the low abundance of NH_4NO_3. For example, a 60% decrease in TNH_3 yields only about a 2 μg m^{-3} reduction in WSICs, and a 60% cut in TNO_3 reduces WSICs by roughly 1.4 μg m^{-3}. By comparison, sulfate control is markedly more efficient: a 60% reduction in sulfate lowers WSICs by approximately 9.5 μg m^{-3}. In winter, higher NH_4NO_3 abundance increases the leverage of both TNO_3 and TNH_3 controls. The marginal efficiency of TNO_3 control rises to about 0.08 μg m^{-3} WSIC reduction per 1% TNO_3 decrease, or roughly 0.85 μg m^{-3} WSIC reduction per 1 μg m^{-3} decrease in TNO_3 (Fig. S12). Sulfate control remains effective but is somewhat less efficient than in fall due to the lower

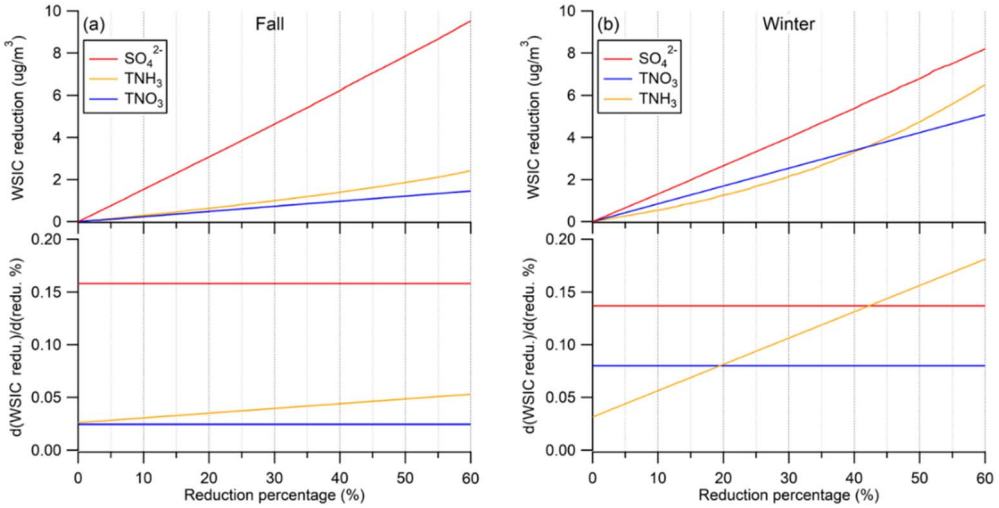

Fig. 8 Efficiency of controlling sulfate, TNO_3, and TNH_3 for reducing total WSIC concentrations during (a) fall and (b) winter. Top panels show WSIC reduction *vs.* the reduction factor for each precursor. Bottom panels show the corresponding derivatives of the lines in the top plots.

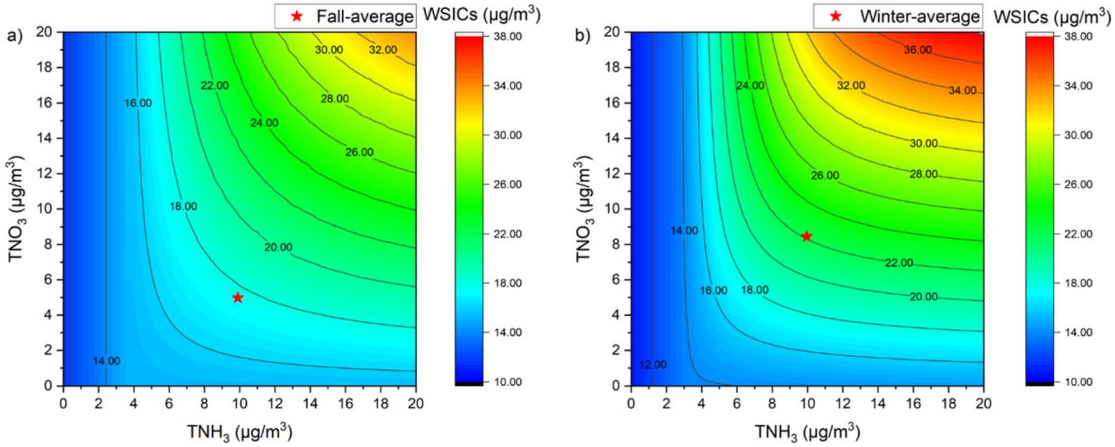

Fig. 9 Simulated WSIC concentrations as functions of TNO_3 and TNH_3 in the range of 0 to 20 μg m^{-3} during (a) fall and (b) winter. The star in each plot denotes seasonal average conditions.

fraction of ammonium sulfate; only about 0.14 μg m^{-3} of WSICs is reduced per 1% decrease in sulfate. For modest reductions (<20% or <2.5 μg m^{-3}), TNH_3 control is less effective than TNO_3 control for lowering WSICs in winter. However, at larger reductions (>45% or ≥4.3 μg m^{-3}), TNH_3 abatement becomes the most efficient of the two semi-volatile pathways (Fig. S12). These results support the feasibility of controlling semi-volatile precursors, TNH_3 and TNO_3, for wintertime PM mitigation, while highlighting sulfate abatement as the dominant WSIC-reduction lever in fall.

Although our single-factor perturbation analyses provide quantitative insights into the individual sensitivity of $PM_{2.5}$ mass to these components, it is important to acknowledge their limitation in capturing the full complexity of real-world emission scenarios. In practice, controls on TNO_3, sulfate and TNH_3 are likely to be implemented simultaneously, and the thermodynamic system response may be non-additive due to strong non-linear interactions. For instance, the $\varepsilon(NO_3^-)$ level is strongly modulated by the ambient NH_3 levels (Fig. S10 and S11), so a coordinated reduction of TNH_3 and TNO_3 would not be additive. Instead, it would drive the system into a regime where the marginal $PM_{2.5}$ reduction per unit of NH_3 cut is greatly amplified, representing a synergistic effect. Quantification of this synergistic effect is analyzed in the following section.

3.5.2 Simulations with simultaneous variation of TNO_3 and TNH_3. We conducted simulations in which TNO_3 and TNH_3 were varied simultaneously from 0 to 20 μg m^{-3} under fixed meteorological conditions and background composition to evaluate seasonal responses of WSICs (Fig. 9). For identical TNO_3–TNH_3 combinations, winter conditions produced slightly higher WSIC concentrations than fall because lower temperatures enhance partitioning of nitrate and ammonium to the particle phase. The contour fields also differed in structure between the two seasons. Fall exhibited more diffuse, widely spaced contours, reflecting weaker PM sensitivity to HNO_3 and NH_3 availability relative to winter, where tighter gradients indicate stronger thermodynamic leverage of these precursors.

Baseline conditions, marked according to seasonal averages in Table 4, lie near the ridge line of the WSIC response surface in both seasons. This placement indicates that reducing either TNO_3 or TNH_3 from current levels is effective in cutting down WSIC concentration, and that concurrent reductions in both precursors provide an even larger benefit. Accordingly, coordinated TNO_3 and TNH_3 controls represent a thermodynamically efficient strategy for mitigating $PM_{2.5}$ during high-pollution seasons, outperforming approaches that target only one of the two semi-volatile precursors.

4. Conclusions

We combined hourly water-soluble ionic species measurements with meteorological data and ISORROPIA-II thermodynamic modeling to characterize aerosol pH and quantify $PM_{2.5}$ mass sensitivity to ammonia and nitrate availability in urban Hong Kong. Using the sensitivity regime framework of Nenes *et al.*,[26] we mapped seasonal regime behaviors and further quantified sensitivities through simulations that reduced total ammonia (TNH_3), total nitrate (TNO_3), and sulfate. Aerosol pH typically ranged from 1.5 to 3 throughout the year. Its diurnal amplitude exceeded seasonal and interannual variability, indicating that meteorology, particularly temperature, exerts stronger control on aerosol acidity than compositional changes under Hong Kong conditions. Winter consistently showed higher pH than other seasons, attributable to lower temperatures.

Pollution episodes were concentrated in fall and winter, but seasonal differences in composition produced distinct sensitivity patterns. In fall, sulfate dominated WSICs, and PM mass was more sensitive to TNH_3 than to TNO_3 availability. In winter, nitrate and ammonium contributed larger mass fractions, yielding enhanced sensitivity to both TNH_3 and TNO_3. Component-wise perturbation analyses clarified these mechanisms. Reducing TNO_3 had negligible effects on aerosol pH or AWC and therefore did not shift PM sensitivity regimes. Reducing TNH_3 increased NH_3 sensitivity while diminishing TNO_3 sensitivity in both seasons by limiting ammonium

availability for NH_4NO_3 formation. Sulfate reductions strengthened TNH_3 sensitivity across seasons by lowering acidity and AWC, with a more pronounced enhancement of TNO_3 sensitivity in winter than in fall, consistent with greater wintertime NH_4NO_3 formation.

Nitrate was primarily present as ammonium nitrate. Most observations fell within the "NH_4^+ rich" regime, where nitrate is neutralized by excess ammonium, and more than 70% of excess ammonium was present as NH_4NO_3. These findings support TNH_3 control as an effective lever for $PM_{2.5}$ mitigation. Efficiency analyses further showed that sulfate abatement reduces WSICs slightly less efficiently in winter than in fall (approximately 0.14 *versus* 0.16 μg m^{-3} per 1% sulfate reduction). By contrast, TNO_3 controls were substantially more effective in winter than in fall due to higher NH_4NO_3 abundance (approximately 0.08 *versus* 0.03 μg m^{-3} WSIC reduction per 1% TNO_3 reduction). Reductions in WSICs exhibited a nonlinear (parabolic) response to TNH_3 abatement; as TNH_3 decreases, the marginal efficiency of control increases. Sulfate always had the highest marginal efficiency in cutting down PM mass during fall, followed by TNH_3 and TNO_3. In winter, the marginal efficiency of TNH_3 reduction would be higher than TNO_3 with a reduction rate of 20%; once TNH_3 reductions exceed about 45%, ammonia control becomes more effective than sulfate in lowering WSICs.

Overall, coordinated reductions of TNH_3 and TNO_3 provide a thermodynamically efficient pathway for $PM_{2.5}$ mitigation during high-pollution seasons, while sulfate abatement remains a robust year-round strategy, especially in fall when sulfate dominates WSICs and nitrate formation is constrained. These results highlight the importance of season-specific, composition-aware control portfolios that target both non-volatile and semi-volatile precursors to optimize $PM_{2.5}$ reductions in urban areas that face similar challenges to those encountered in Hong Kong.

Conflicts of interest

There are no conflicts to declare.

Data availability

Data for this article, including raw sampling data and simulation results, are available at: https://dataspace.hkust.edu.hk/bib/JKV87K.

Supplementary information (SI): figures. See DOI: https://doi.org/10.1039/d5ea00114e.

Acknowledgements

This work was partly supported by the Research Grants Council of Hong Kong (R6011-18). We thank the Hong Kong Environmental Protection Department for provision of the real-time $PM_{2.5}$ and MARGA datasets. The content of this paper does not necessarily reflect the views and policies of the HKSAR Government, nor does mention of trade names or commercial products constitute an endorsement or recommendation of their use.

References

1 X. H. H. Huang, Q. Bian, W. M. Ng, P. K. K. Louie and J. Z. Yu, Characterization of $PM_{2.5}$ Major Components and Source Investigation in Suburban Hong Kong: A One Year Monitoring Study, *Aerosol Air Qual. Res.*, 2014, **14**(1), 237–250.

2 W. S. Chow, K. Liao, X. Huang, K. F. Leung, A. K. Lau and J. Z. Yu, Measurement Report: Ten-year trend of PM 2.5 major components and source tracers from 2008 to 2017 in an urban site of Hong Kong, China, *Atmos. Chem. Phys.*, 2022, 1–24.

3 G. John J. C. C. Watson, X. Wang and D. Steven, *Kohl Hong Kong Fine Particulate Matter (PM2.5) Chemical Compositions*, 2021.

4 J. Zhen Yu and T. Zhang, *Final Report for Chemical Speciation of PM2.5 Filter Samples*, January 1 through December 31, 2017, 2018.

5 B. J. Gu, L. Zhang, R. Van Dingenen, M. Vieno, H. J. M. Van Grinsven, X. M. Zhang, S. H. Zhang, Y. F. Chen, S. T. Wang, C. C. Ren, S. Rao, M. Holland, W. Winiwarter, D. L. Chen, J. M. Xu and M. A. Sutton, Abating ammonia is more cost-effective than nitrogen oxides for mitigating PM2.5 air pollution, *Science*, 2021, **374**(6568), 758.

6 M. Liu, X. Huang, Y. Song, J. Tang, J. Cao, X. Zhang, Q. Zhang, S. Wang, T. Xu, L. Kang, X. Cai, H. Zhang, F. Yang, H. Wang, J. Z. Yu, A. K. H. Lau, L. He, X. Huang, L. Duan, A. Ding, L. Xue, J. Gao, B. Liu and T. Zhu, Ammonia emission control in China would mitigate haze pollution and nitrogen deposition, but worsen acid rain, *Proc. Natl. Acad. Sci. U. S. A.*, 2019, **116**(16), 7760–7765.

7 A. Pozzer, A. P. Tsimpidi, V. A. Karydis, A. de Meij and J. Lelieveld, Impact of agricultural emission reductions on fine-particulate matter and public health, *Atmos. Chem. Phys.*, 2017, **17**(20), 12813–12826.

8 A. Ismaeel, A. P. K. Tai and J. Wu, Understanding the spatial patterns of atmospheric ammonia trends in South Asia, *Sci. Total Environ.*, 2024, **954**, 176118.

9 K. E. Wyer, D. B. Kelleghan, V. Blanes-Vidal, G. Schauberger and T. P. Curran, Ammonia emissions from agriculture and their contribution to fine particulate matter: A review of implications for human health, *J. Environ. Manage.*, 2022, **323**, 116285.

10 L. Liu, W. Xu, X. Lu, B. Zhong, Y. Guo, X. Lu, Y. Zhao, W. He, S. Wang, X. Zhang, X. Liu and P. Vitousek, Exploring global changes in agricultural ammonia emissions and their contribution to nitrogen deposition since 1980, *Proc. Natl. Acad. Sci. U. S. A.*, 2022, **119**(14), e2121998119.

11 T. Huai, T. D. Durbin, J. W. Miller, J. T. Pisano, C. G. Sauer, S. H. Rhee and J. M. Norbeck, Investigation of NH3 emissions from new technology vehicles as a function of vehicle operating conditions, *Environ. Sci. Technol.*, 2003, **37**(21), 4841–4847.

12 D. C. Carslaw and G. Rhys-Tyler, New insights from comprehensive on-road measurements of NOx, NO2 and

NH3 from vehicle emission remote sensing in London, UK, *Atmos. Environ.*, 2013, **81**, 339–347.
13 S. M. Griffith, X. H. H. Huang, P. K. K. Louie and J. Z. Yu, Characterizing the thermodynamic and chemical composition factors controlling $PM_{2.5}$ nitrate: Insights gained from two years of online measurements in Hong Kong, *Atmos. Environ.*, 2015, **122**, 864–875.
14 Y. Cheng, G. Zheng, C. Wei, Q. Mu, B. Zheng, Z. Wang, M. Gao, Q. Zhang, K. He and G. Carmichael, Reactive nitrogen chemistry in aerosol water as a source of sulfate during haze events in China, *Sci. Adv.*, 2016, **2**(12), e1601530.
15 M. Liu, Y. Song, T. Zhou, Z. Xu, C. Yan, M. Zheng, Z. Wu, M. Hu, Y. Wu and T. Zhu, Fine particle pH during severe haze episodes in northern China, *Geophys. Res. Lett.*, 2017, **44**(10), 5213–5221.
16 T. Tan, M. Hu, M. Li, Q. Guo, Y. Wu, X. Fang, F. Gu, Y. Wang and Z. Wu, New insight into $PM_{2.5}$ pollution patterns in Beijing based on one-year measurement of chemical compositions, *Sci. Total Environ.*, 2018, **621**, 734–743.
17 G. Shi, J. Xu, X. Peng, Z. Xiao, K. Chen, Y. Tian, X. Guan, Y. Feng, H. Yu, A. Nenes and A. G. Russell, pH of Aerosols in a Polluted Atmosphere: Source Contributions to Highly Acidic Aerosol, *Environ. Sci. Technol.*, 2017, **51**(8), 4289–4296.
18 M. Zhou, G. Zheng, H. Wang, L. Qiao, S. Zhu, D. Huang, J. An, S. Lou, S. Tao and Q. Wang, Long-term trends and drivers of aerosol pH in eastern China, *Atmos. Chem. Phys.*, 2021, 1–21.
19 J. Xue, A. K. H. Lau and J. Z. Yu, A study of acidity on $PM_{2.5}$ in Hong Kong using online ionic chemical composition measurements, *Atmos. Environ.*, 2011, **45**(39), 7081–7088.
20 R. J. Weber, H. Guo, A. G. Russell and A. Nenes, High aerosol acidity despite declining atmospheric sulfate concentrations over the past 15 years, *Nat. Geosci.*, 2016, **9**(4), 282–285.
21 A. S. Wexler and S. L. Clegg, Atmospheric aerosol models for systems including the ions H^+, NH_4^+, Na^+, SO_4^{2-}, NO_3^-, Cl^-, Br^-, and H_2O, *J. Geophys. Res.: Atmos.*, 2002, **107**(D14), ACH 14.
22 A. Stelson and J. Seinfeld, Relative humidity and temperature dependence of the ammonium nitrate dissociation constant, *Atmos. Environ.*, 2007, **41**, 126–135.
23 M. Michael, The dissociation constant of ammonium nitrate and its dependence on temperature, relative humidity and particle size, *Atmos. Environ.*, 1993, **27**(2), 261–270.
24 Z. Meng and J. H. Seinfeld, Time scales to achieve atmospheric gas-aerosol equilibrium for volatile species, *Atmos. Environ.*, 1996, **30**(16), 2889–2900.
25 A. Stelson and J. Seinfeld, Relative humidity and pH dependence of the vapor pressure of ammonium nitrate-nitric acid solutions at 25 C, *Atmos. Environ.*, 1982, **16**(5), 993–1000.
26 A. Nenes, S. N. Pandis, R. J. Weber and A. Russell, Aerosol pH and liquid water content determine when particulate matter is sensitive to ammonia and nitrate availability, *Atmos. Chem. Phys.*, 2020, **20**(5), 3249–3258.
27 Q. Zhao, A. Nenes, H. Yu, S. Song, Z. Xiao, K. Chen, G. Shi, Y. Feng and A. G. Russell, Using High-Temporal-Resolution Ambient Data to Investigate Gas-Particle Partitioning of Ammonium over Different Seasons, *Environ. Sci. Technol.*, 2020, **54**(16), 9834–9843.
28 C. Fountoukis and A. Nenes, ISORROPIA II: a computationally efficient thermodynamic equilibrium model for K^+–Ca^{2+}–Mg^{2+}–NH_4^+–Na^+–SO_4^{2-}–NO_3^-–Cl^-–H_2O aerosols, *Atmos. Chem. Phys.*, 2007, **7**(17), 4639–4659.
29 H. Guo, A. P. Sullivan, P. Campuzano-Jost, J. C. Schroder, F. D. Lopez-Hilfiker, J. E. Dibb, J. L. Jimenez, J. A. Thornton, S. S. Brown, A. Nenes and R. J. Weber, Fine particle pH and the partitioning of nitric acid during winter in the northeastern United States, *J. Geophys. Res.: Atmos.*, 2016, **121**(17), 10355–10376.
30 C. J. Hennigan, J. Izumi, A. P. Sullivan, R. J. Weber and A. Nenes, A critical evaluation of proxy methods used to estimate the acidity of atmospheric particles, *Atmos. Chem. Phys.*, 2015, **15**(5), 2775–2790.
31 H. Guo, L. Xu, A. Bougiatioti, K. M. Cerully, S. L. Capps, J. R. Hite, A. G. Carlton, S. H. Lee, M. H. Bergin, N. L. Ng, A. Nenes and R. J. Weber, Fine-particle water and pH in the southeastern United States, *Atmos. Chem. Phys.*, 2015, **15**(9), 5211–5228.
32 J. I. Steinfeld, Atmospheric chemistry and physics: from air pollution to climate change, *Environ.: Sci. Policy Sustainable Dev.*, 1998, **40**(7), 26.
33 W. S. Chow, X. H. H. Huang, K. F. Leung, L. Huang, X. Wu and J. Z. Yu, Molecular and elemental marker-based source apportionment of fine particulate matter at six sites in Hong Kong, China, *Sci. Total Environ.*, 2022, **813**, 152652.
34 J. Li, Q. Liu, Y. Li, T. Liu, D. Huang, J. Zheng, W. Zhu, M. Hu, Y. Wu and S. Lou, Characterization of aerosol aging potentials at suburban sites in northern and southern China utilizing a potential aerosol mass (Go: PAM) reactor and an aerosol mass spectrometer, *J. Geophys. Res.: Atmos.*, 2019, **124**(10), 5629–5649.
35 Y. K. Wong, K. M. Liu, C. Yeung, K. K. Leung and J. Z. Yu, Measurement report: Characterization and source apportionment of coarse particulate matter in Hong Kong: insights into the constituents of unidentified mass and source origins in a coastal city in southern China, *Atmos. Chem. Phys.*, 2022, **22**(7), 5017–5031.
36 Q. Ying, J. Li and S. H. Kota, Significant Contributions of Isoprene to Summertime Secondary Organic Aerosol in Eastern United States, *Environ. Sci. Technol.*, 2015, **49**(13), 7834–7842.
37 H. O. Pye, R. W. Pinder, I. R. Piletic, Y. Xie, S. L. Capps, Y. H. Lin, J. D. Surratt, Z. Zhang, A. Gold, D. J. Luecken, W. T. Hutzell, M. Jaoui, J. H. Offenberg, T. E. Kleindienst, M. Lewandowski and E. O. Edney, Epoxide pathways improve model predictions of isoprene markers and reveal key role of acidity in aerosol formation, *Environ. Sci. Technol.*, 2013, **47**(19), 11056–11064.
38 World Health Organization, *WHO Global Air Quality Guidelines: Particulate Matter (PM2.5 and PM10), Ozone, Nitrogen Dioxide, Sulfur Dioxide and Carbon Monoxide*, World Health Organization, Geneva, p. 2021.
39 J. P. S. Wong, Y. Yang, T. Fang, J. A. Mulholland, A. G. Russell, S. Ebelt, A. Nenes and R. J. Weber, Fine

Particle Iron in Soils and Road Dust Is Modulated by Coal-Fired Power Plant Sulfur, *Environ. Sci. Technol.*, 2020, **54**(12), 7088–7096.

40 Y. Tao, X. Ye, Z. Ma, Y. Xie, R. Wang, J. Chen, X. Yang and S. Jiang, Insights into different nitrate formation mechanisms from seasonal variations of secondary inorganic aerosols in Shanghai, *Atmos. Environ.*, 2016, **145**, 1–9.

41 R. K. Pathak, W. S. Wu and T. Wang, Summertime PM 2.5 ionic species in four major cities of China: nitrate formation in an ammonia-deficient atmosphere, *Atmos. Chem. Phys.*, 2009, **9**(5), 1711–1722.

42 K. He, Q. Zhao, Y. Ma, F. Duan, F. Yang, Z. Shi and G. Chen, Spatial and seasonal variability of PM2.5 acidity at two Chinese megacities: insights into the formation of secondary inorganic aerosols, *Atmos. Chem. Phys.*, 2012, **12**(3), 1377–1395.

43 Y.-C. Lin, Y.-L. Zhang, M.-Y. Fan and M. Bao, Heterogeneous formation of particulate nitrate under ammonium-rich regimes during the high-PM2.5 events in Nanjing, China, *Atmos. Chem. Phys.*, 2020, **20**(6), 3999–4011.

44 X. Huang, R. Qiu, C. K. Chan and P. Ravi Kant, Evidence of high PM2.5 strong acidity in ammonia-rich atmosphere of Guangzhou, China: Transition in pathways of ambient ammonia to form aerosol ammonium at $[NH_4^+]/[SO_4^{2-}]$ =1.5, *Atmos. Res.*, 2011, **99**(3–4), 488–495.